Experimental and Numerical Study of Ceramic Foam Filtration

E. Laé[1], H. Duval[2], C. Rivière[1,2], P. Le Brun[1], J.-B. Guillot[2]

[1.] Alcan Centre de Recherches de Voreppe, 725 rue Aristide Bergès,
BP 27, 38341 Voreppe Cedex, France
[2.] Laboratoire de Génie des Procédés et Matériaux, École Centrale Paris,
Grande Voie des Vignes, 92295 Châtenay-Malabry, France

Keywords: Ceramic foam filter, Depth filtration, Inclusions, Lattice-Boltzmann model.

Abstract

Ceramic foam filtration is widely used to enable removal of non metallic inclusions from liquid aluminium. Its performances have been largely studied in the literature and some discrepancies remain amongst the published results. Consequently, a research program was deployed to evaluate the performances of a range of ceramic foam filters used under various conditions and to understand the inclusions capture mechanisms.
On the first hand, laboratory trials were run on a filtration pilot under carefully controlled thermal and hydrodynamic conditions. The filtration efficiency of the Ceramic Foam Filter (CFF) was assessed by LiMCA measurements. Microscopic observations of the filter still impregnated with solidified metal were also carried out to know the repartition of the inclusions within the filter as well as their capture sites.
On the other hand, the initial filtration efficiency as well as the inclusion capture sites were calculated by a two-dimension lattice-Boltzmann filtration model [1] on several types of ceramic foam filters, for various types of inclusion. Results of this work are presented and discussed.

Introduction

The performance requirements for aluminium alloys are continually increasing, in particular with regard to inclusion removal. Indeed, the presence of non-metallic inclusions in alloys affects the quality and properties of the products in many different ways. Therefore, filtration of the melt has been introduced into the process in order to remove inclusions and thus meet high quality standards. Liquid aluminium is usually filtered through ceramic foam filters, granular beds or rigid media filters.
Ceramic foam filters have been largely studied in the literature; their performances are reviewed here. The techniques used to evaluate them are varied: metallographic observations of a filter section after use, PoDFA, LAIS and LiMCA measurements. Particular emphasis is laid on the use of LiMCA and metallographic observations since they are the two techniques used for this study. The filtration efficiency is used as an evaluation criterion of the CFF, it is defined by equation (1)

$$E = \frac{N20_i - N20_0}{N20_i} * 100 \quad (1)$$

Where N20i is the average N20 LiMCA index at the filter inlet and N20o is the average N20 LiMCA index at the filter outlet. The figure 1 gives a summary of the filtration efficiency evaluated by LiMCA measurements before and after the filter in function of the filter grade and the filtration parameters (filtration speed and alloy) reported by previous papers [2-9]. The filtration speed is defined by equation (2)

$$v = \frac{Q}{\rho S} \quad (2)$$

Where Q is the mass flow rate, ρ is the molten aluminium density and S the filter surface.
The figure 1 shows the wide range of CFF efficiencies from 30-60% efficiency to 80-90% efficiency. It is believed the different parameters under which the CFF are used can explain these discrepancies.
Indeed, the influence of various parameters on the CFF efficiency was also studied, they can be classified between the filter parameters (pore size and chemistry), the inclusions parameters (nature, size and number) and the process parameters (alloy, use of grain refining rod, filtration speed, upstream treatment).
It was shown that the filtration efficiency increases when the pore size decreases [3] or when the grade in ppi increases [10,2].
The filtration efficiency is supposed to be larger for larger inclusions [2,10]. However a decrease in efficiency for inclusion size decreasing from 20 to 50µm was shown in some cases [9,5]. It is attributed to inclusions agglomeration in the CFF. Dupuis et al. [9] showed an increase of efficiency with the increase of the incoming inclusion concentration. The filtration efficiency is shown to be a decreasing exponential function of the filter depth [9,11], typical of depth filtration.
A decrease of the filtration speed increases the filtration efficiency [9,12,13] and some brutal variations of speed can cause inclusions release [9]. The use of grain refining rod at the filter inlet was shown to decrease the filtration efficiency of a 50ppi filter, the effect being significative in the case of high inclusions loading (N15 around 10k/kg) [14].
Most studies giving efficiency values based on LiMCA measurements report metallographic observations of spent filters. Several papers [5,6] showed that the inclusion content was decreasing in quantity from the top to the bottom. The formation of bridges across the ceramic foam window in the uppermost part of the filter was also evidenced [2,5,14]. High filtration efficiency could be related to a cake filtration occurring thanks to these bridges. The bridges are more numerous when the filter is fine and when there is no grain refining added. The main filtration mode of the CFF is supposed to be depth filtration [9,15].
The results present in the literature show some disagreements on the filtration mechanisms and the influence of various parameters on filtration efficiency.
The present study gives an input on how the different parameters impact filtration efficiency and what are the filtration mechanisms. Filtration modeling is also used to evaluate the influence of these parameters. As a discussion, experimental and numerical results are compared.

J. F. Grandfield and D. G. Eskin (Eds.), *Essential Readings in Light Metals*

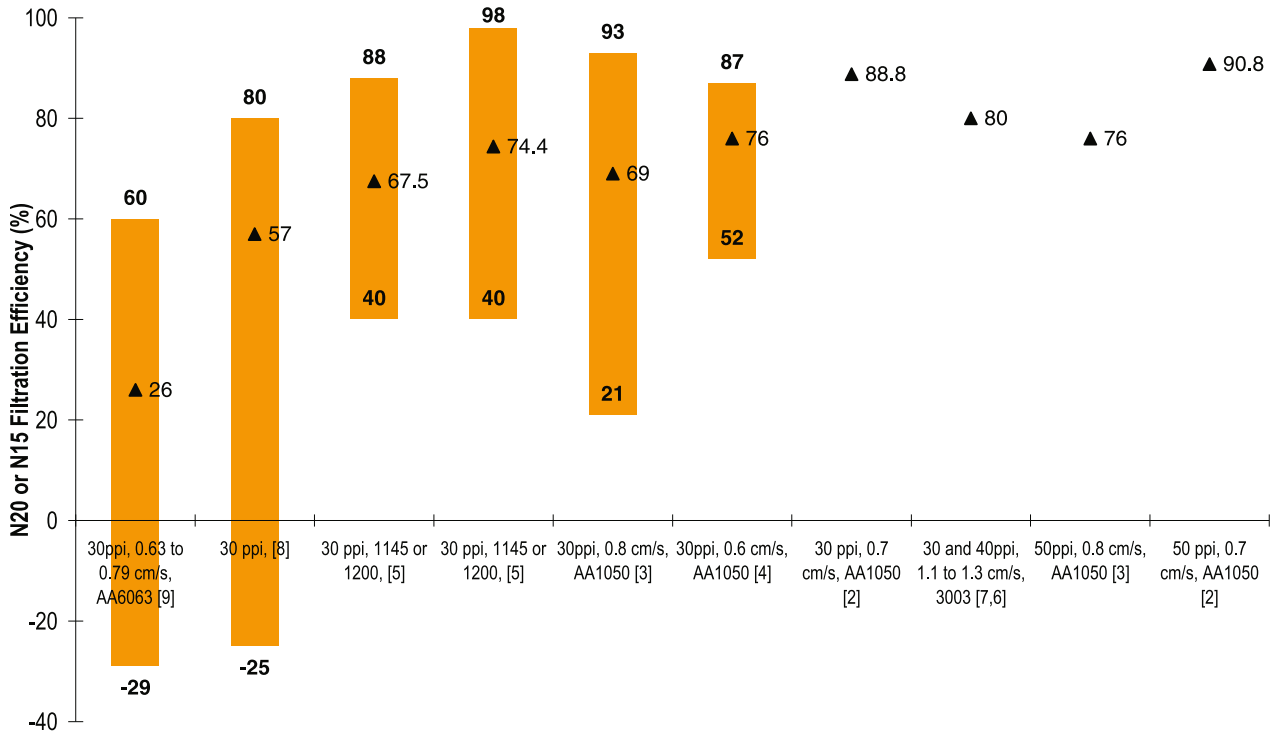

Figure 1. Filtration efficiencies in function of the filter grade (reference 3 and 4, efficiency measured on N15, rest: N20)

Experimental Details

A filtration pilot was designed in order to study the filtration efficiency of different filters used under various conditions. It is represented on figure 2.

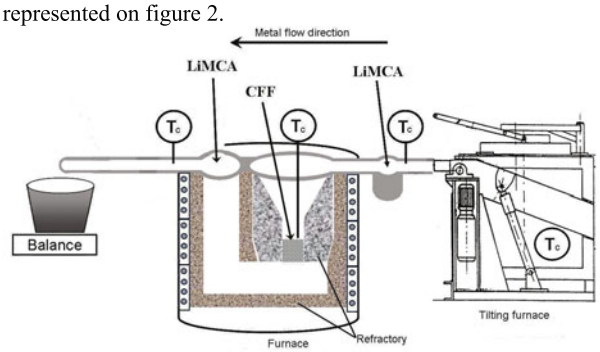

Figure 2. Filtration pilot principle scheme

The filtration pilot is made of a resistance tilting furnace, a launder system, a resistance furnace and a metal recuperation ladle.
The ceramic foam filter is cut into cylinders to fit into a refractory mould. The filtration module is held into the resistance furnace. The casting line is instrumented with three thermocouples, one before the filter, one after the filter and the last one on the tile.

Two scale experiments were done. The main parameters are summarized in table I.

Table I. Characteristics of the two scale experiments

	configuration 1	configuration 2
tilting furnace capacity (kg)	70	700
filter diameter (mm)	50	100
casting time (min)	10 to 20	40 to 70

The standard experimental procedure was the following. The alloy is elaborated in the tilting furnace, the charges are made of aluminium ingots and raw materials. The filter is impregnated and the cast starts. The metal is poured regularly into the launder, through the filter and to the recuperation ladle. The metal flow rate is measured continuously thanks to a balance placed under the recuperation ladle. Thermal conditions were reproducible. For the molten metal characterization, LiMCA are used before and after the filter. Once the cast is over, the filter solidifies in the AET furnace.

The first advantage of this experimental setup is the fact that the metal can calmly solidify in the filter without being touched. For most industrial ceramic foam filters, the tile is drained of metal after the cast, which makes direct observation difficult. Furthermore, the tile undergoes shocks to be removed of its seat, which is thought to create inclusions releases. Thanks to this setup, the inclusions present in the tile stay at the location where they were trapped. Consequently, the tile could be cut longitudinally and transversally for metallographic observations of the inclusions at various heights.
The second advantage is that proper LiMCA measurements can be done before and after the filter. In most plants, this type of measurements does not give the right inclusion concentration in molten metal because of the degassing treatment occurring just

before the CFF. The micro bubbles present in molten metal are seen by the LiMCA as inclusions. The use of an extension probe or measuring during the pressure cycle is supposed to reduce the amount of gas bubbles seen by the LiMCA. However, it was shown that these two techniques underestimate the inclusion concentration and the problem of interpreting LiMCA particles count in the presence of micro bubbles is still unresolved [16]. Consequently, this experimental set up enables the evaluation of the filtration efficiency of the CFF only. For these trials, the LiMCA measurements were exploited to calculate the average filtration efficiency for the inclusions larger than 20, 40 and 60 microns.

Various trials were done to study the influence of the following parameters on filtration efficiency: the alloy (including 1080 or 5182), the tile grade (including 30ppi or 50ppi), the grain refining presence, the particles size, the filtration speed.

Numerical tools

A depth filtration model using the lattice-Boltzmann method was developed [1] and a standard procedure was defined. A flow chart summarizes it in figure 3.

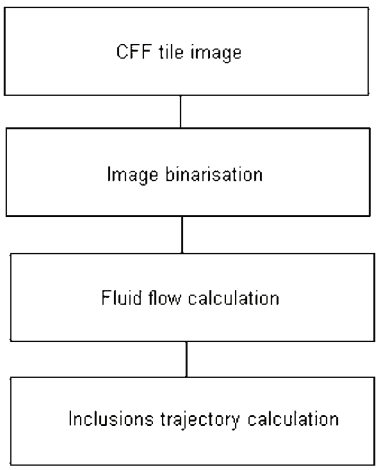

Figure 3. Flow chart of the depth filtration model

The filter image can be obtained by impregnating a tile piece in black resin, by polishing it and by digitalizing it.
The binary image is obtained thanks to image analysis software.
The model first module calculates the fluid flow within the filter according to the process parameters (filtration speed or head loss). The post-treated data are: the streamlines, the velocity vectors and the pressure at every point of the fluid, the head loss. An example is given on figure 4.
The model second module calculates the inclusion trajectory. The parameters are the inclusion size, density and number, the adhesion force. The post-treated data are the map of the initial capture probability density and the initial filtration efficiency. The initial filtration efficiency is defined by the filtration efficiency at the beginning of the cast, when the filter is clean.

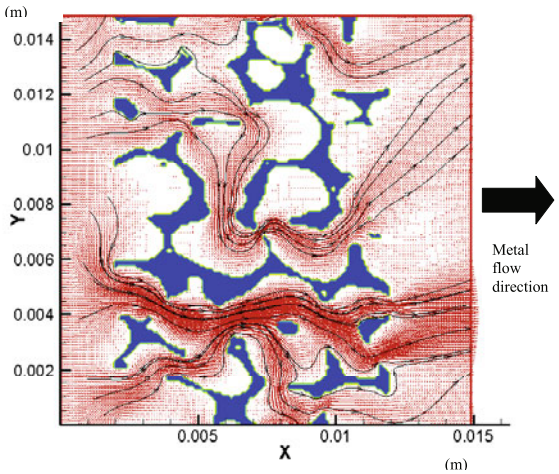

Figure 4. Velocity vectors and streamlines on a 30ppi filter, the filtration speed is 0.3 cm/s

A preliminary study was done to define a representative elementary surface of a ceramic foam filter. Starting from digital images of whole ceramic foam filters, calculations were done on various computational domains. The size varied from 1500 nods width and 1000 to 4707 nods height, the resolution being 10µm. The inclusions were 50 µm large and their densities varied from 2200 to 3900 kg/m3.
It was verified that the filtration efficiency follows the exponential law of equation 3 as reported in [9,11].

$$E_0 = 1 - \exp(-\lambda_0 L) \qquad (3)$$

Eo is the initial filtration efficiency, λo is the initial filtration coefficient and L is the filter thickness.
The results are shown in figure 5.

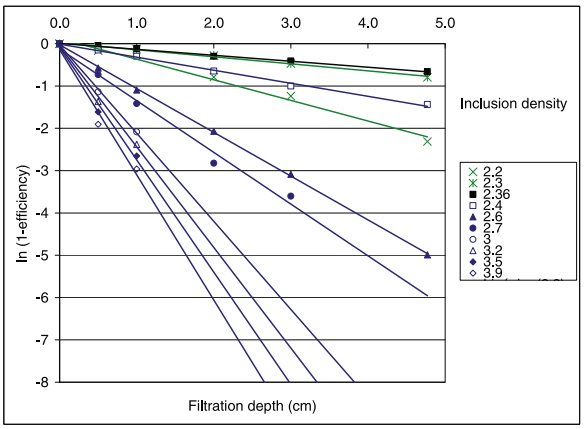

Figure 5. Representation of ln (1-Efficiency) in function of the filter depth for a range of inclusions densities

The initial filtration coefficient can be deduced of the figure 5 and calculations can be done on a domain of 1000*1500 nods, the resolution being 10µm.

Results

Typical LiMCA curves obtained on the filtration pilot are represented on figure 6.

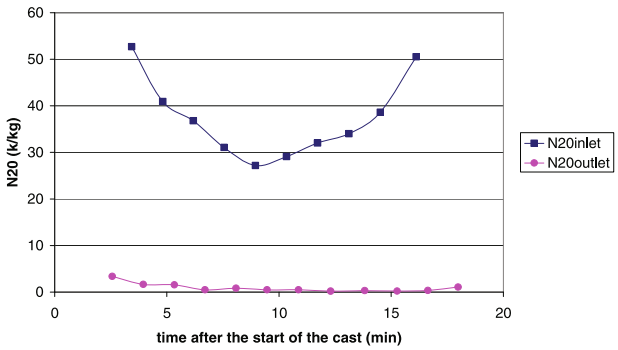

Figure 6. Example of LiMCA measurements done at the 30ppi filter inlet and outlet, 1080 alloy, 0.73 cm/s

The figure 6 shows that the filtration pilot is relevant since the phenomena occurring in plants at the furnace outlet and at the filter outlet are present. First, the settling of the particles in the furnace occurs at the beginning of the cast. At the end of the cast, when the furnace is emptied, an increase in the N20 is due to the settling of the particles in the furnace heel. Furthermore, inclusion releases can be generated by metal flow instabilities as they occur on industrial filters [9].

The efficiencies measured on the filtration pilot varied between 50% and 98% depending on the parameters used. This range is close to the efficiency range found in figure 1. A few cases are presented here.
On the alloy 5182, with a filtration speed of 1.3 cm/s, the LiMCA measurements done before and after a 30ppi from supplier A give an average filtration efficiency of 80% on the N20 and N40 and 85% on the N60 as shown on figure 7.

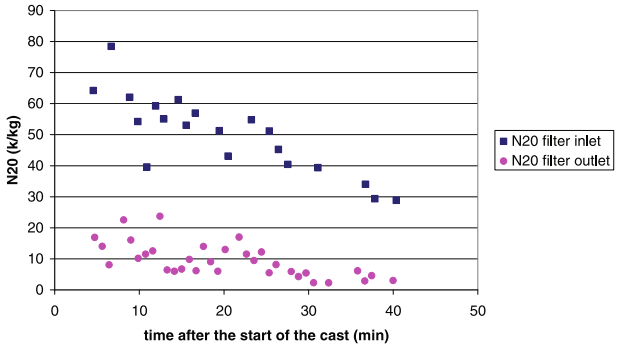

Figure 7. Efficiency of a 30ppi filter measured by LiMCA

On the alloy 5182, with a filtration speed of 1.8 cm/s, the efficiency of a 50ppi filter from supplier B is 62% for the N20, 55% for the N40 and 63% for the N60 as shown on figure 8.
It is interesting to note that despite the finer porosity, the efficiency is less important for the 50ppi filter. This is thought to be due to the higher filtration speed and also to the fact that the filters come from different suppliers. It was shown that the morphology of the filters closely related to filtration efficiency varies a lot with the supplier even for the same grades expressed in ppi [17].

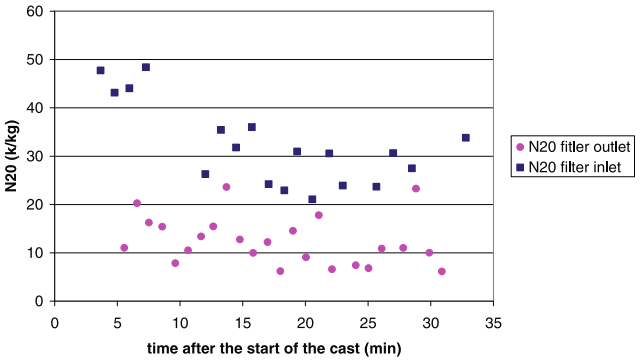

Figure 8. Efficiency of a 50ppi filter measured by LiMCA

The model is useful to decorrelate the effects of filtration speed and tile grade on filtration efficiency.
A sensitivity study was done to study the influence of filtration speed on filtration efficiency. It was verified on a standard case that the filtration efficiency decreases when the filtration speed increases. The results are presented on figure 9. The literature and industrial trends are consequently well represented by the model. The study of the inclusions capture sites shows that the higher the filtration speed, the deeper the inclusions penetrate into the filter.

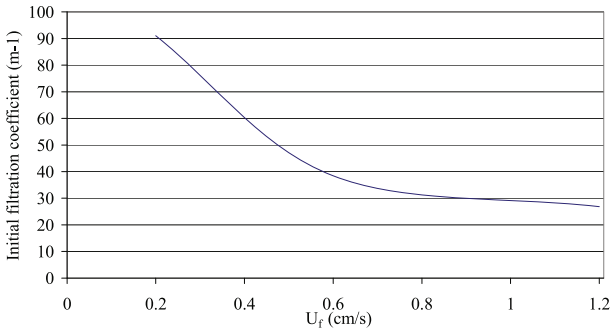

Figure 9. Computed influence of filtration speed on initial filtration coefficient (60ppi filter, 50µm-3200 kg/m3 inclusions)

A sensitivity study was also done on the filter grade. It was shown that for a same supplier, the initial filtration coefficient is proportional to the specific perimeter of the filter, characteristic of a filter type (grade and supplier) measured by image analysis. The results are presented on figure 10.

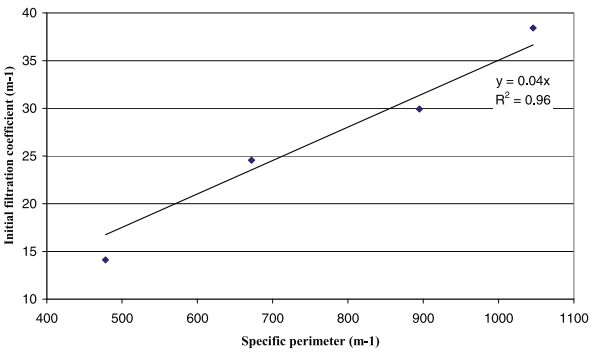

Figure 10. Computed relation between initial filtration coefficient and specific perimeter

This result shows the importance of the specific parameter to characterize the filters rather than the grade.

The model was run with the parameters conditions of figure 7. Initial filtration efficiencies were calculated for magnesium oxide and alumina inclusions of 50µm diameter. These inclusions were found to be the most numerous stopped by the filter. The results found were respectively 71% and 85%. The experimental filtration efficiency was 77%. These figures are in good agreement.

The repartition of the inclusions on the height of some filters was studied. The inclusions were localized and counted on transverse cuts of a quarter of the filter. A typical image is represented on figure 11. On this filter for example, 160 metallographic cuts were observed and the repartition of the inclusions on the filter height is represented on figure 12. It shows that the inclusions are mainly trapped in the first millimetres of the filter. The figure 12 shows that the repartition profile of the inclusions is a decreasing exponential profile. It is possible to deduce the filtration efficiency in function of the filter height z. The figure 13 represents ln (1-efficiency(z)) in function of z. The curve can be fitted by a straight line. The filtration occurred in a deep bed mode [9,11].

Figure 11. Transversal metallographic cut of a quarter of the filter (100µm from the filter inlet)

The comparison between figure 5 and figure 13 shows that the filtration law relating efficiency and the filter height are of the same form. The filtration mode is consequently well represented by the model. A closer examination of the inclusion capture sites calculated by the model show that the main inclusion trapping mechanisms are sedimentation and interception. The inclusions stopped by sedimentation are localized in zones where the local metal speed is low.
However some phenomena were shown experimentally to have an impact on filtration but are not represented by the model yet.

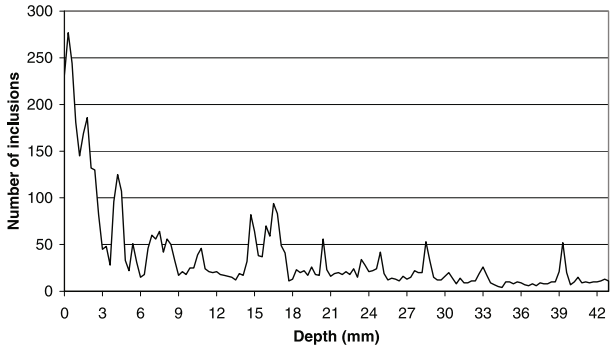

Figure 12. Repartition of the inclusions on the filter height

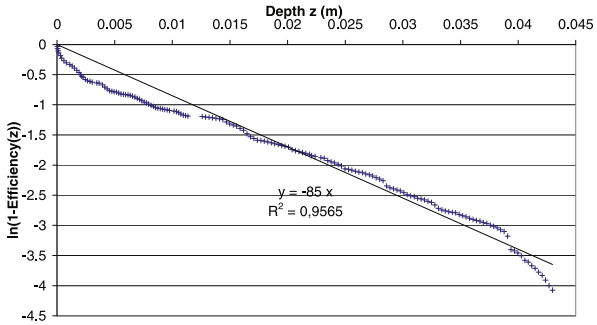

Figure 13. Filtration law linking filtration efficiency and filter depth

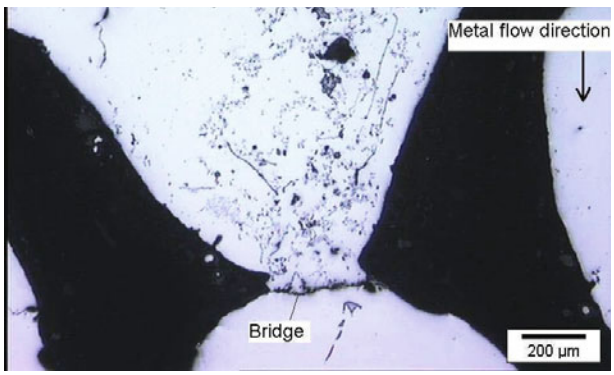

Figure 14. Presence of an oxide bridge at the filter inlet stopping the inclusions

First the metallographic observations showed that oxide skins are present near the surface of the filter on a depth of 2mm, they form bridges that decrease the size of the windows or even close them as shown on figure 14. A proposed filtration mechanism is that the bridges formed by the oxide skins play the part of a net for the incoming inclusions as shown on figure 14. These observations are consistent with the published work [6,7,10,15].
The influence of grain refining rod was studied in alloy 5182, on a 50ppi filter at a 1.8 cm/s filtration speed. AT5B was introduced after 12 minutes of casting for 20 minutes, at a rate of 1kg/t. The point of AT5B introduction was after the LiMCA measuring at the filter inlet so that the LiMCA inlet level was not affected by the AT5B introduction. The average N20 at the filter inlet were 33 k/kg and 29 k/kg respectively before and after the AT5B introduction. The average N20 at the filter outlet

increased from 9k/kg to 20k/kg when refining rod is introduced. This result is shown on figure 15. In terms of filtration efficiency, it decreases from 73% to 31% when grain refining rod is added.

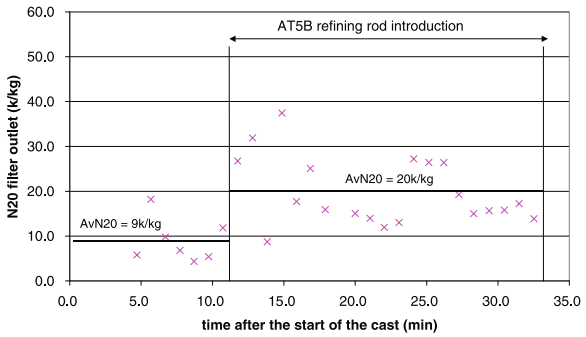

Figure 15. Influence of grain refining addition on the filter outlet level

The impact of grain refining rod on filtration efficiency had already been studied in AA1050 alloy [14]. The same phenomena as the one illustrated on figure 15 occurred when grain refining rod was added. The presence of grain refiner was supposed to prevent the formation of bridges in the filter. The same phenomena may occur in 5182 alloy since the high magnesium content enhances the formation of oxide skins involved in the formation of bridges.

Conclusions

A filtration pilot was designed to study the influence of various parameters on filtration efficiency measured by LiMCA and to do metallographic analysis of the filters after use. The LiMCA measurements show that the pilot is representative of industrial conditions. Some cases were presented where the combination of a higher filtration speed and a thinner porosity can lead to a lower efficiency than the one got with a lower filtration speed and a coarser porosity.

A filtration model using the lattice Boltzmann method was used to study separately the sensitivity of filtration speed and grade. The industrial trends are well represented. The specific perimeter is shown to be a key characteristic of the filter morphology linked to efficiency.

On a macroscopic point of view, some experimental and numerical results match in terms of filtration efficiency. On a microscopic point of view, the analysis of used filters show that the repartition of the inclusions on the filter height follows an exponential law characteristic of depth filtration, this is also well represented by the model.

The presence of oxide skins in the filter was evidenced as well as their role as inclusion trapping nets whereas the model foresees trapping of inclusions by sedimentation and direct interception. The role of grain refining rod on the decrease of filtration efficiency in a 5182 alloy was evidenced. The formation of bridges and their interaction with grain refining particles could be implemented in the model to improve it.

Acknowledgments

This research was supported the Ministère de l'Économie, des Finances et de l'Industrie of France, as part of the CIPAL project. E. Waz, J. Trubuil, R. Rey Flandrin and Y. Pouyet are greatly acknowledged for their technical contribution to the project.

References

1. C. Rivière., H. Duval, J-B.Guillot, *2D lattice-Boltzmann model of aluminium depth filtration*, Light Metals, 2004, pp. 761-766.
2. S. Instone, M. Badowski, W. Schneider, *Development of molten metal filtration technology for aluminium*, Light Metals, 2005, pp. 933-938.
3. N. J. Keegan, W. Schneider, H. P. Krug, V. Dopp, *Evaluation of the efficiency of ceramic foam and bonded particle cartridge filtration system*s, Light Metals, 1997, pp. 973-982.
4. W. Schneider, H P Krug, N. J. Keegan, *Efficiency and Performance of Industrial Filtration Systems*, Sixth Australasian Asian Pacific Conference on Aluminium Casthouse Technology, 1999, pp. 159-174.
5. D. D. Smith, L.S. Aubrey, W.C. Miller, *LiMCA II evaluation of the performance characteristics of single element and staged ceramic foam filtration,* Light Metals, 1998, pp. 893-915.
6. L. A. Strom, J. W. Black, R. I. L Guthrie, C. Tian, *Non-ferrous alloy filtration efficiency study of fully sintered reticulated ceramics utilizing LiMCA and LAIS*, Light Metals, 1992, pp. 1093-1100.
7. C. Tian, R.I.L. Gutrie, *Rheological aspects of liquid metal filtration using reticulated ceramic foam filters*, Light Metals, 1993, pp. 1003-1007
8. C. Dupuis, R. Dumont, *Impact of LiMCA technology on the optimization of metal cleanliness*, Light Metals, 1993, pp. 997-1002.
9. C. Dupuis, G. Béland, JP. Martin, *Filtration Efficiency of Ceramic Foam Filters for production of high quality molten aluminium alloys*, Proceedings of the 32nd annual conference of metallurgists, (Québec, Canada, CIM, 1993), pp. 349-358
10. N. J. Keegan, W. Schneider, H. P. Krug, *Evaluation of the efficiency of fine pore ceramic foam filters*, Light Metals 1999, pp. 1031-1041.
11. R. Mutharasan, D. Apelian, A. Romanowski, *A laboratory investigation of aluminum filtration through deep-bed and ceramic open-pore filters*, J. of Metals, 1981, vol. 33(12), pp. 12-18
12. D. Apelian, R. Mutharasan, *Filtration : a melt refining method*, J. of Metals, 1980, vol. 32(9), pp. 14-19.
13. C. Conti, *Contribution à l'étude de la filtration profonde des métaux*, PhD thesis, 1983, Faculté Polytechnique de Mons, 294 pages.
14. N. Townsey, W. Schneider, H.P. Krug, A. Hardman, N.J. Keegan, *The influence of grain refiners on the efficiency of ceramic foam filters*, Light Metal, 2001, pp. 973-977.
15. L.S. Aubrey, J.E. Dore, *Ceramic Foam – a deep bed or caking filter in aluminium cast shop operations*, Light Metals, 1993, pp. 1009-1020.
16. M. Cooksey, T. Ware, M.J. Couper, *Effect of pressure cycle and extension probe on LiMCA measurement of inclusions*, Light Metals, 2001, pp. 965-971.
17. B. Milligan, S. F. Ray, *Recent improvements in the measurement and control of ceramic foam filter quality*, Proc. Int. Conf. Advances in Production and Processing of Aluminum (APPA 2001), 2001, Manama, Bahrain, 15 pages.